2012

Process planning and control of functionally graded parts using freeze-form extrusion fabrication

Bradley Kenneth Deuser

Department:

Recommended Citation

Deuser, Bradley Kenneth, "Process planning and control of functionally graded parts using freeze-form extrusion fabrication" (2012). *Masters Theses*. 7350.
https://scholarsmine.mst.edu/masters_theses/7350

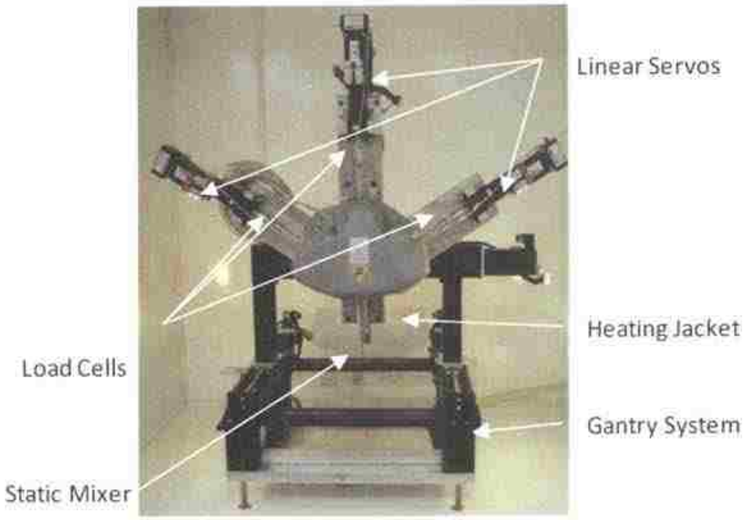

Figure 1: FEF machine with triple extruder mechanism.

Freeze-form Extrusion Fabrication (FEF) is a novel, layer-by-layer additive manufacturing process that builds three-dimensional (3D) parts by extruding aqueous-based colloidal pastes in an environment below the freezing point of water (-10° in our present study) in order to solidify the material as it exits the nozzle. This increases the build strength of each part and allows the FEF process to fabricate parts larger than that of room temperature extrusion processes (e.g., Robocasting [5] and Fab@Home [6]), and enables unsupported overhangs as much as 35° from the horizontal surface [7]. The triple-extruder FEF machine is capable of depositing three separate pastes from a single orifice by using an inline static mixer to blend together multiple materials (Figure 2). This passive mixing technique has been used to minimize the number of moving components and controller complexity. However, it introduces a transport delay for changes in material composition that must be taken into account by the path planning software.

Figure 2: Static mixer (left) with mixing elements (right).

The research detailed in this paper outlines key issues for fabricating parts with multiple materials using the triple-extruder FEF system, which include: development of a general tracking velocity controller for the extrusion servo motors, taking into account the transport delay caused by the static mixer, and applying compositional gradients to

Table 1: Linear cylinder parameters

Cylinder	τ (s)	*K* (mm/s/V)	*f* (mm/s)
1	$3.60 \cdot 10^{-3}$	11.95	0.934
2	$4.82 \cdot 10^{-3}$	11.81	1.056
3	$4.26 \cdot 10^{-3}$	11.62	1.022

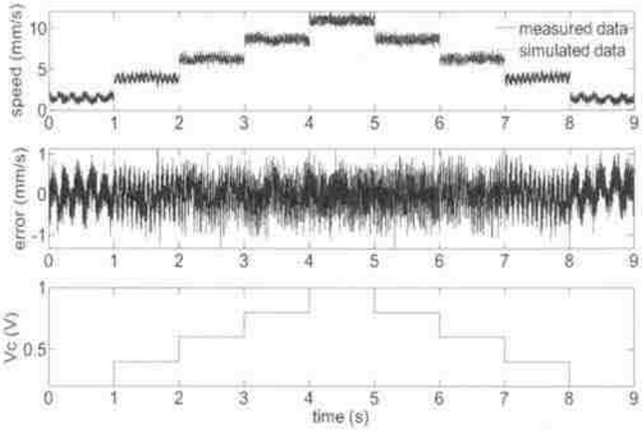

Figure 4: Comparison of the linear cylinder 1 velocity model and experimental results

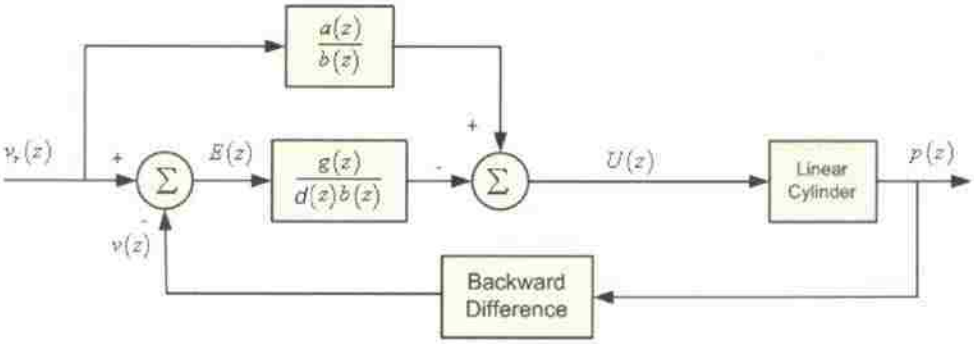

Figure 5: General tracking velocity controller

Here,

$$\frac{V(z)}{U(z)} = \frac{k\left(1-e^{-T/\tau}\right)}{z-e^{-T/\tau}} = \frac{b(z)}{a(z)} \tag{2}$$

and $d(z) = z - 1$ in Figure 5 is the disturbance-generating polynomial. By including this polynomial, the Internal Model Principle is utilized to robustly reject constant

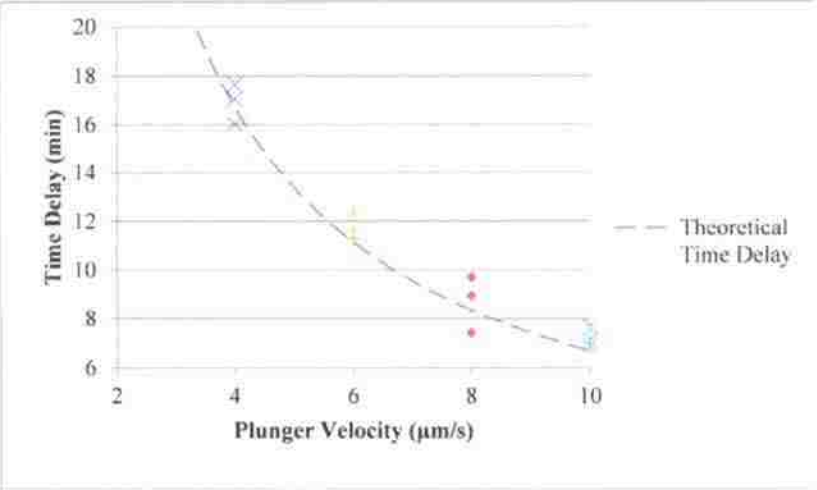

Figure 6: Experimental validation of the time delay model at four plunger velocities

The experimental results yield good accuracy for each plunger velocity when compared to the analytical predictions. For each velocity, the average of three runs comes within <4% of the theoretical time delay. One important factor in successful time delay repeatability is to ensure that the paste has been pre-loaded, or compressed, at the steady state force in each syringe prior to extrusion. For example, at a plunger velocity of 10 μm/s, the time delay averages seven minutes. When the target material was not pre-loaded to the steady state force (typically 600 N) prior to extrusion, delay times of up to fifteen minutes were observed. This increased delay has been thought to occur because the paste being used has some degree of compressibility which allows material from one syringe to enter the other if the two syringes are not both pre-loaded to an equal force. This compressibility also adds error to the time delay measurements if the paste is not pre-loaded, by introducing a transient phase to the initial startup as the force ramps up to a steady state value. For continuous extrusion, this issue can be solved by maintaining a steady extrusion force for both cylinders. However, planning of tool paths for extrusion on demand (EOD), as required for most motion code programs must take this compressibility into account to avoid lengthening the time delay and facing the consequence of materials switching at an undesired location.

5. CONTROL OF MATERIAL GRADIENTS

The algorithm developed to control the material gradient has two main functions: 1) implementing compensation for material transport delay and 2) applying material composition gradients to existing tool path motion code for homogeneous materials. The cylinder shown in Figure 7 was built by manually changing the velocity of each plunger to achieve a gradient from green to pink limestone ($CaCO_3$) paste in increments of 10% composition. In this case, G-code was written manually using circular arc functions, and the time delay was calculated and tested manually by varying the velocity of each plunger. The composition was varied by 10% every ten layers from the bottom (green) to the top (pink). It can be observed that composition increments near 10% for this height achieve a nearly continuous gradient over short distances from one material to the next. The goal of the gradient control algorithm is to automate this process for any geometry. In order to make the algorithm more versatile, it was designed to take in tool path information from both the Stratasys Insight software and generic G&M code to apply the transport delay and material gradients. With this functionality, primitive shapes such as plate or bar test specimens can be coded manually in G&M code and loaded into the program to apply the gradient and transport delay without having to model these simple shapes and go through the slicing and conversion process.

Figure 7: Cylinder with vertical gradient

5.1. Program Overview

The program was written in Mathworks Matlab 8, and its operation is outlined in Figure 8. It first reads in a text file output from Stratasys Insight, which includes tool path information in the format of Categorical Abstract Machine Language (CAML). Because motion control is executed through Delta Tau PEWIN software, tool path information must be translated into G&M coding language. Commands such as table speed (feed rate), extrusion status (on/off), and motion commands in the absolute positioning domain are extracted and converted. The resulting code is then modified to include Extrusion on Demand (EOD) commands and varying composition gradients by

layer of the test bar (4 mm in height), where the base layer is composed of 100% paste A and each subsequent layer contains a region to the right of 100% A (pink) and a region to the left of 100% B (green). Horizontal gradients showed repeatability from layer to layer within 1 cm in either direction for a total of eight layers. As mentioned previously, the transition region makes up 15-30% of the total time delay; therefore one limitation of the inline static mixer is a required minimal length for each layer in order to be able to fully transition from one material to the next. On average, for a plunger velocity of 10 µm/s, transitional mixing has been observed to take place in 81 cm or less. Since the overall length for each layer shown in Figure 11 is 203 cm, and 40% of the time extruding material is spent transitioning between paste A and paste B, only 30% of the part is pure A and 30% is pure B. This effect is undesirable for small parts, but larger parts may see some benefit from this transitional zone. For example, if two pastes composed of materials with different shrinkage rates are used to build a part, this transitional mixing will act as a buffer between composition changes to reduce the risk of delamination during the freeze-drying and sintering stages of post-processing. The pre-defined gradient could obviously be tailored such that drastic composition changes are avoided, but transitional mixing may add another level of protection to the green part and such complicated gradient schemes would not be necessary.

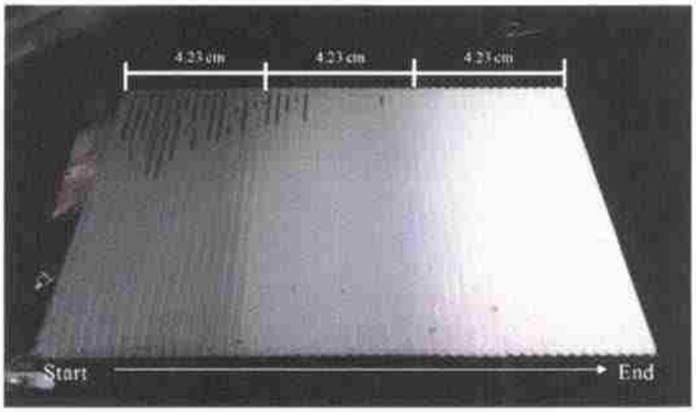

Figure 10: Transition from Al_2O_3 (gray) to Al_2O_3 (white), including a 50% mixing

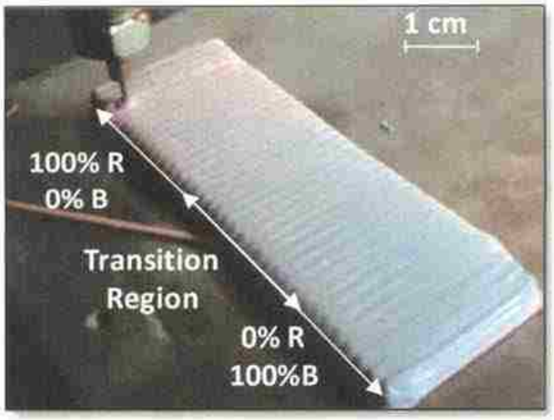

Figure 11: Eight-layer 2.54 cm by 10 cm block as the test bar.

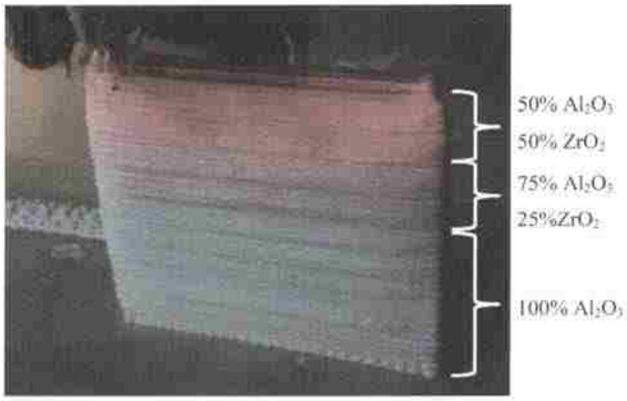

Figure 12: Alumina/Zirconia composite test part.

5.3.2. G-code interpretation for Vertical Gradients. The vertical test bar shown in Figure 12 was produced using two pastes: 100% Alumina (paste A) and 50%Alumina-50%Zirconia (paste B). These tests were conducted to ensure the resulting mixture of paste A and paste B was of the correct composition. This part was built in an environment of -10°C from manually written G-code and automatically generated velocity control to vary the composition from 100% paste A (100%Al_2O_3) for the first 20 layers to 50% paste A and 50% of paste B (75%Al_2O_3-25%ZrO_2) for the next 10 layers and 100% paste B (50%Al_2O_3-50%ZrO_2) for the final 10 layers. The part was freeze dried, sintered, cut and polished before applying a gold/palladium coating to condition the part for energy dispersive x-ray spectroscopy (EDS) measurements. Control pellets were manually mixed in precise measurements from the same alumina and alumina/zirconia pastes and sintered for comparison to the 75%Al_2O_3-25%ZrO_2 mixture to ensure the correct composition was being achieved. EDS intensity measurements verified that the mixture of the two pastes mixed and

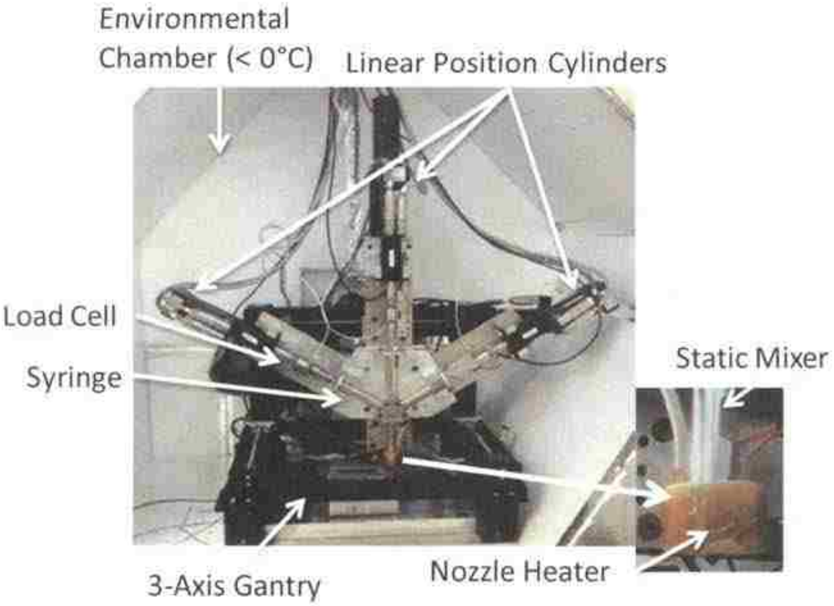

Figure 1: FEF System Setup.

This mixing technique blends together multiple pastes into a homogeneous mixture; however, it introduces a transport delay into the system, denoted t_d. The transport delay is modeled using linear relationships between the paste volumetric flow rate Q (mm^3/s) and the internal volume of the static mixer V (mm^3) as follows:

$$t_d = \frac{V}{\sum_{i=1}^{n} Q_i} = \frac{V}{A_1 v_1 + A_2 v_2 + A_3 v_3} \tag{1}$$

where $n = 3$ is the number of cylinders being used, A_i is the cross sectional area of the i^{th} cylinder (mm^2), and v_i is the velocity of the i^{th} plunger (mm/s). The volumetric flow rate from all three extruders, Q, is equal to the sum of the flow rates from the individual cylinders, Q_1, Q_2, and Q_3. The ratio of these three flow rates represents the ratio of the three pastes; therefore, the composition ratio is controlled by regulating the velocity of each plunger, as illustrated in Figure 2.

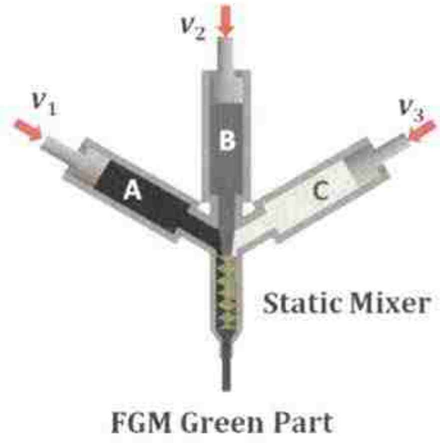

Figure 2: Triple extruder mechanism for static mixing of up to three colloidal pastes to form an FGM part.

The FEF system is comprised of two coupled mechatronic systems (Figure 3). Extrusion is controlled with three Kollmorgen servo motors (N2 Series AKM23D) using a Servostar300 series amplifier and a National Instruments PXI chassis with LabVIEW Real Time. Each servo motor drives a linear position cylinder and the encoders are sampled by a counter/timer card (PXI-6602) run in quadrature mode, and a first order finite difference scheme is utilized to achieve a velocity resolution of 0.2 μm/s. Each linear cylinder is equipped with a load cell (Omega LC-305) to track the amount of force being exerted on a stainless steel plunger, which is housed in a stainless steel syringe. The load cells have a maximum load rating of 4448 N and a resolution of 7 N. The load cell signals are sampled through a PXI-6025E multifunction card with an A/D resolution of 12 bits at a maximum sampling rate of 200 kS/s and an input range of ±10 V. Command voltages are sent to the servo motor amplifiers through a PXI-6711 high-speed analog output card, which has a 12-bit D/A resolution, a maximum sampling rate of 1MS/s and a voltage range of ±10 V.

The three-axis gantry system is controlled using a Delta Tau Turbo PMAC card, which operates the FEF machine through NC G&M motion code via PEWIN 32 software. The two systems are coupled by sending analog signals from the Delta Tau system to the PXI-6025E LabVIEW multifunction board and an A/D converter.

$$V_c(k) = V_c(k-1) + \frac{u_{ref}(k+1) - \left(1 + e^{-T_s/\tau_u}\right)u_{ref}(k) - e^{-T_s/\tau_u}u_{ref}(k-1)}{K_u\left(1 - e^{-T_s/\tau_u}\right)} - \frac{g_1 e_u(k) + g_0 e_u(k-1)}{K_u\left(1 - e^{-T_s/\tau_u}\right)} \quad (5)$$

where u_{ref} (mm/s) is the reference plunger velocity and the plunger velocity error is

$$e_u(k) = u_{ref}(k) - u_p(k) \quad (6)$$

The general tracking plunger velocity controller is tested using a reference plunger velocity pyramid step input from 2 to 10 μm/s (Figure 6). The noise observed in this figure is from two sources: 1) operating near the minimum velocity range of the linear cylinders (1 μm/s) and 2) using a first order backward finite difference method to estimate the plunger velocity. The steady-state error is approximately ±2 μm/s after filtering the data using a first order low-pass filter with a cut-off frequency of 40 Hz.

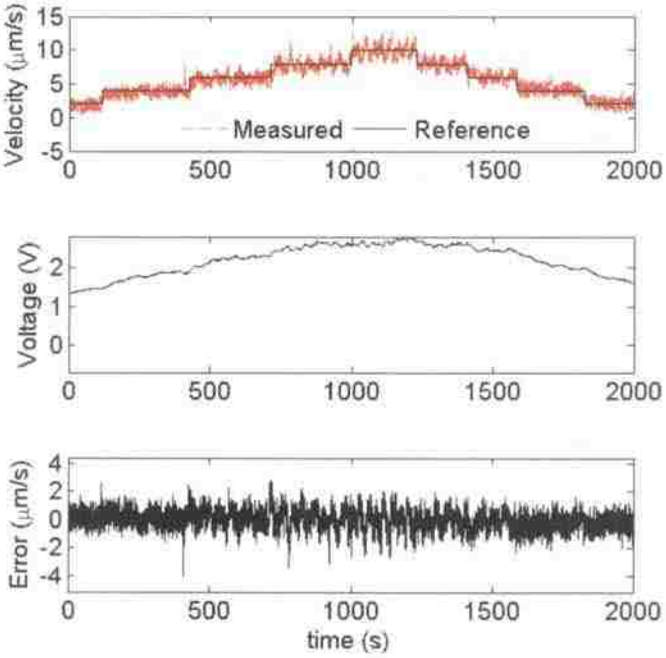

Figure 6: Plunger velocity controller response to a pyramid step input reference velocity trajectory.

4. EXTRUSION FORCE MODELING AND CONTROL

Since the extrusion force is directly correlated to the steady-state and transient behavior of the extrudate velocity, an extrusion force controller is developed to compensate for the slow extrudate velocity response to changes in plunger velocity. Fast

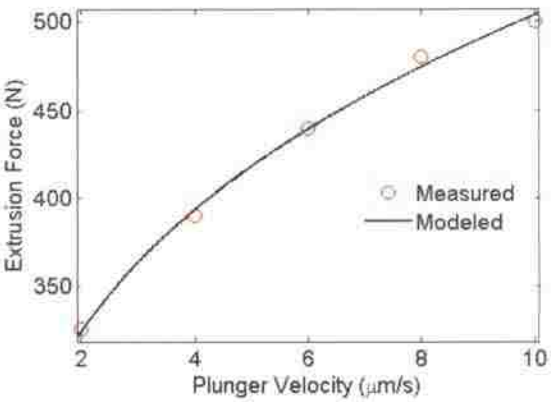

Figure 7: Measured and modeled steady-state extrusion forces.

The dynamic extrusion force model is simulated with a step input plunger velocity of 4 to 10 μm/s and compared to the measured extrusion force in Figure 8. The volume of air within the paste is impractical to measure for each batch of paste; therefore, the volume of air is estimated based on empirical data by observing the difference between the measured and simulated dynamic extrusion force responses and adjusting the estimated volume of air such that the simulation and experimental results match for the first step in plunger velocity. The results match for the first step in plunger velocity when the approximate air volume is 1.4% of the total volume of paste within the syringe (i.e., an air layer thickness of 0.9 mm). The initial pressure within the syringe p_0 is calculated from the initial measured extrusion force. At 218 Pa, this "preload" represents the initial pressure of the paste within the syringe and the minimum pressure required to completely fill the nozzle and initiate extrusion. The simulation's initial conditions are matched to the initial conditions of the experiment.

For the simulation in Figure 8, the extrusion force model resulted in modeling errors within ±20 N, which is approximately three times that of the load cell resolution. An exception is the drop in force at 720 s, which can be attributed to an air bubble release. The open-loop time constant decreases from 56 s to 22 s as the plunger velocity increases 2 to 10 μm/s and the extrusion force increases from 330 to 500 N. The time constant then gradually increases to 59 s as the plunger velocity is reduced from 10 to 2 μm/s.

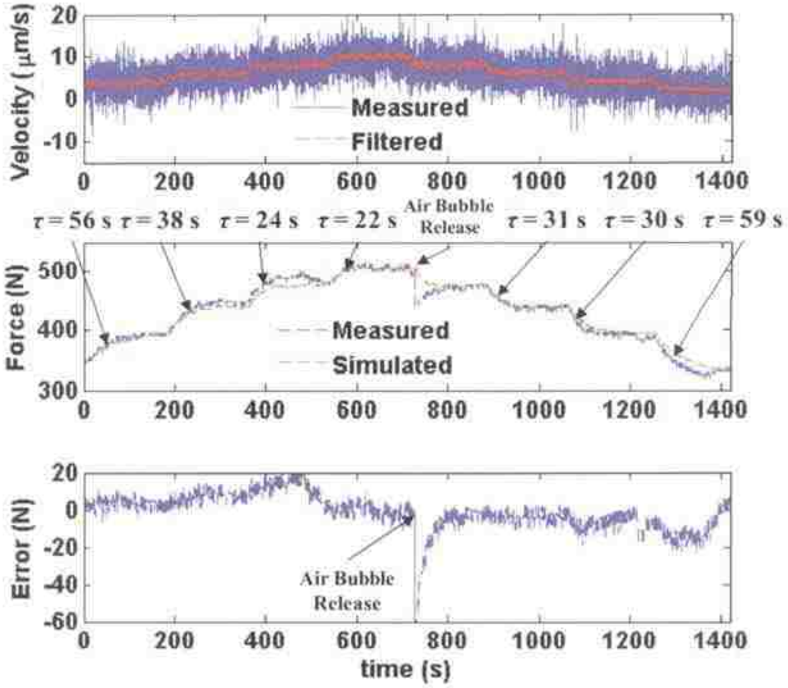

Figure 8: Simulated and measured extrusion forces for $p_0 = 218$ Pa and $l_0 = 0.9$ mm. An air bubble release occurs at 720 s.

4.2. Dynamic Extrusion Force Model Linearization

In order to have robust tracking of the extrusion force, a linearized model-based feedback controller is implemented. The nonlinear model presented in Equation 7 is linearized as follows:

$$g = \dot{f}_L(t) \approx g\left(\overline{f}_L, \overline{u}_p, t\right) + a\left[u_p(t) - \overline{u}_p\right] + b\left[f_L(t) - \overline{f}_L\right] \tag{9}$$

$$a = \left.\frac{\partial g}{\partial f_L}\right|_{\overline{u}_p, \overline{f}_L} = \frac{\left(\overline{f}_L - f_f + A_p P_{atm}\right)^2}{A_p P_0 l_0}\left[-\frac{\varepsilon}{\beta}\left(\frac{\overline{f}_L + \alpha}{\beta}\right)^{\varepsilon - 1} \cdot 10^{-6}\right] \tag{10}$$

$$b = \left.\frac{\partial g}{\partial u_p}\right|_{\overline{u}_p, \overline{f}_L} = \frac{\left(\overline{f}_L - f_f + A_p P_{atm}\right)^2}{A_p P_0 l_0} \tag{11}$$

where $\overline{f}_L$ is the nominal extrusion force (N) and $\overline{u}_p$ is the nominal plunger velocity (m/s). The incremental linearized model is

$$\tau_L \dot{\hat{f}}_L(t) + \hat{f}_L(t) = K_L \hat{u}_p(t) \tag{12}$$

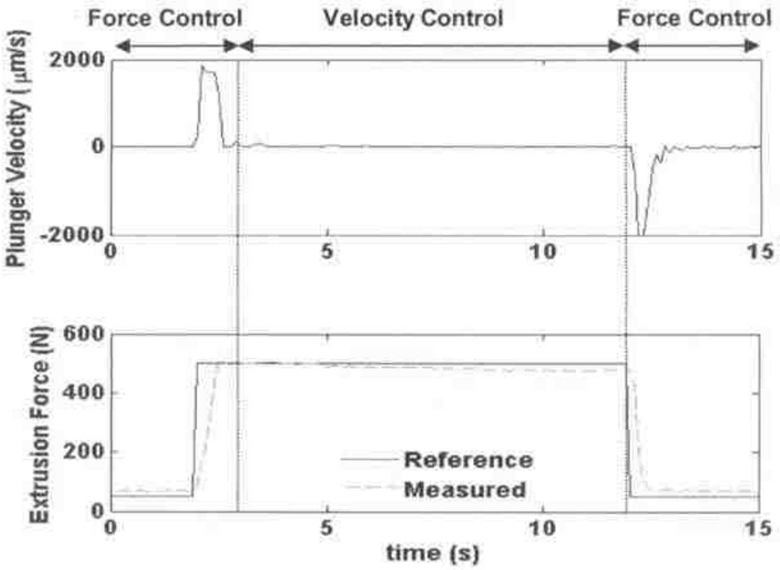

Figure 12: Plunger velocity and extrusion force responses for step change in extrusion force reference from 50 to 500 N to start extrusion and from 500 to 50 N to stop extrusion.

5.2. Dwell-Based Start and Stop Method

Extrusion on demand using a dwell-based method works by positioning the extrusion nozzle at the desired start or stop location and pausing motion for a certain amount of time after issuing a "start" or "stop" command before proceeding to the next motion command. The dwell-based method is investigated by depositing a series of three 12.7 mm paths (Figure 13). Upon receiving a command to start extrusion, the controller is given a step reference extrusion force of 500 N and dwells for a set amount of time (100 to 600 ms) before depositing each segment. Once commanded to stop, the controller sets the reference extrusion force to 50 N and dwells for 100 to 600 ms (Figure 13a). The stop dwell time is assessed by similarly dwelling at the end of each extrusion line before moving to the next line (Figure 13b). This figure shows that it is feasible to use the dwell method for "start" commands since the extrudate track width remained visually consistent, with no thinning or excessive build up of the paste. The optimal dwell time was between 400 and 500 ms. Stop dwell is ineffective because paste continues to exit the nozzle for approximately 100 ms after the command is issued and causes material to build up. Therefore, a trajectory-based method is investigated to cease extrusion before the end of a segment.

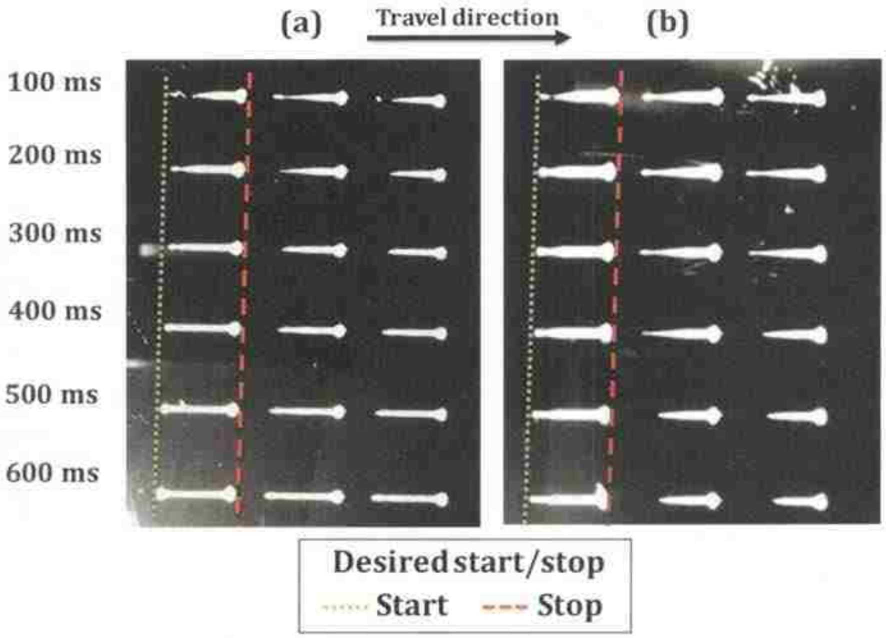

Figure 13: Extrusion segment deposition using the dwell-based method. (a) Dwell start from 100 to 600 ms at the beginning of each segment with 200 ms stop dwell and (b) Dwell stop from 100 to 600 ms at the end of each segment with 200 ms start dwell.

5.3. Trajectory-Based Start and Stop Method

The trajectory-based method issues a "start" or "stop" command to the extruder before the desired start or stop point. This method is tested for start commands by initiating extrusion from 100 to 400 ms before the initial segment point is reached (Figure 14a) and for stop commands by retracting the plunger from 20 to 100 ms before the final segment point is reached (Figure 14b). Trajectory start serves as a validation for the delay time, which is 400 ms for both trajectory and dwell-based start methods. Trajectory stop is capable of producing a constant extrusion track width, with no excessive build-up. Approximately 20 to 40 ms is required to stop extrusion. Longer delay times cause the extrudate track to stop short before the end of the segment, whereas shorter delay times cause build up at the end of the segments.

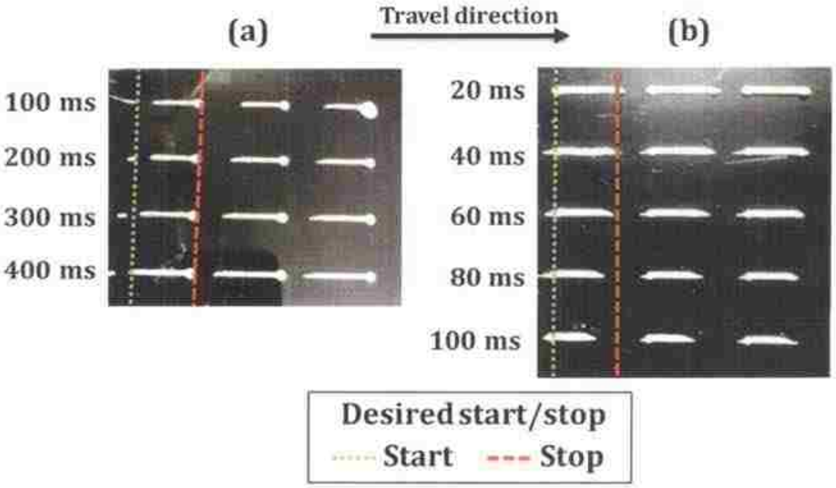

Figure 14: Extrusion segment deposition using trajectory-based method. (a) Early start from 100 to 400 ms ahead of time with 400 ms stop dwell and (b) Early stop from 20 to 100 ms ahead of time with 400 ms start dwell.

5.4. Air Bubble Release Compensation

An added benefit of using a hybrid force-velocity controller is the ability to minimize defects caused by the release of an entrapped air bubble during part fabrication. This capability is evaluated by injecting an air bubble (approximately 1 ml) into the paste. A serpentine pattern is deposited onto a solid substrate until air bubble release occurs. If a velocity controller is utilized, the recovery period after the air bubble releases exhibits a slow first order response, as illustrated in Figure 15a. This causes a sudden spike in the velocity, caused by rapid depressurization, a jump in the plunger position, and a sudden drop in the extrusion force. In this case, the drop in the extrusion force is 50 N and it takes approximately 18 s to reach the original extrusion force since the reference plunger velocity remains constant. During this time, a large gap defect occurs in the deposited material as seen in Figure 16a. The extrusion force controller can minimize gaps formed from air bubble release by adjusting the reference plunger velocity to maintain a constant force on the plunger (Figure 15b). Increasing the reference plunger velocity compensates for the volume lost to the expansion of the air bubble, resulting in a much shorter gap defect as seen in Figure 16b.

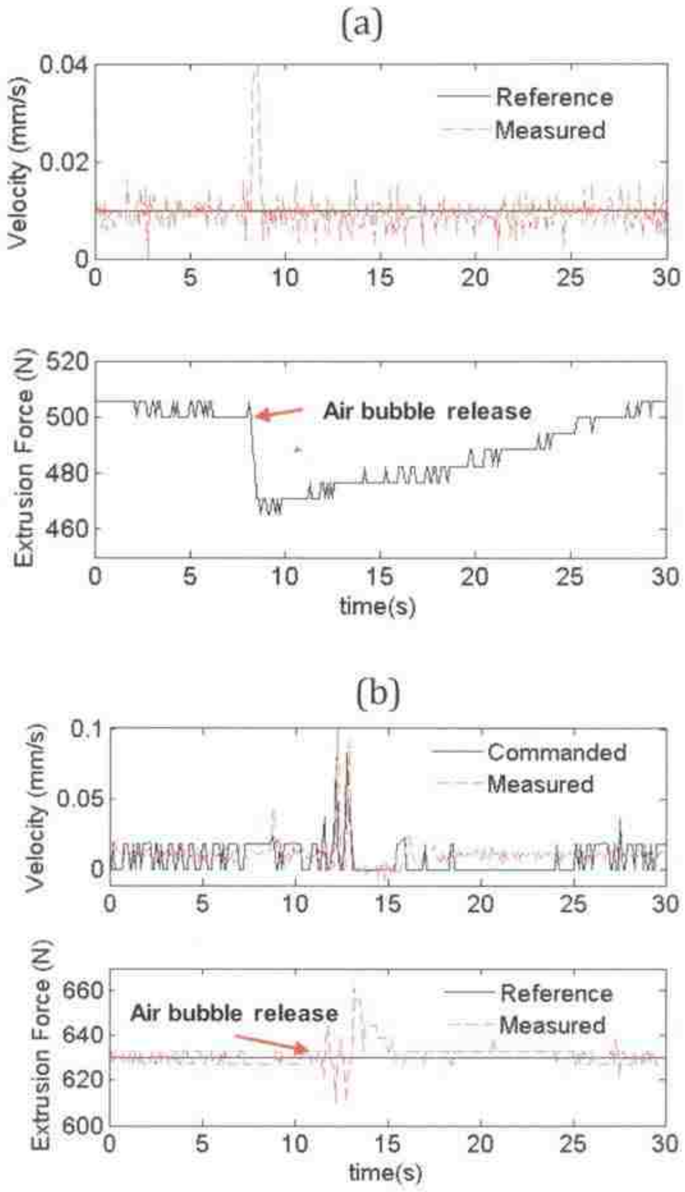

Figure 15: Experimental plunger velocity and extrusion force responses to an air bubble release for (a) velocity controller with $u_{ref} = 0.01$ mm/s and (b) extrusion force controller with $F_{ref} = 630$ N.

(a) (b)

Figure 16: Parts with gap defects caused by an air bubble release for (a) velocity controller with $u_{ref} = 0.01$ mm/s and (b) extrusion force controller with $F_{ref} = 630$ N.

Following an air bubble release, the output flow rate is reduced when using the plunger velocity controller, which may result in a gap defect or a thin extrusion track width until the extrusion force rises back to the steady-state extrusion force. Both cases can be seen in Figure 17a. Gap defects of 2-4 mm are observed and a thinned track width follows one air bubble release, affecting 60 mm of extrudate length. The extrusion force controller responds within 100 ms and the resulting defect is less than 0.5 mm in length, nearly undetectable after the subsequent track fills in a major portion of the gap (Figure 17b).

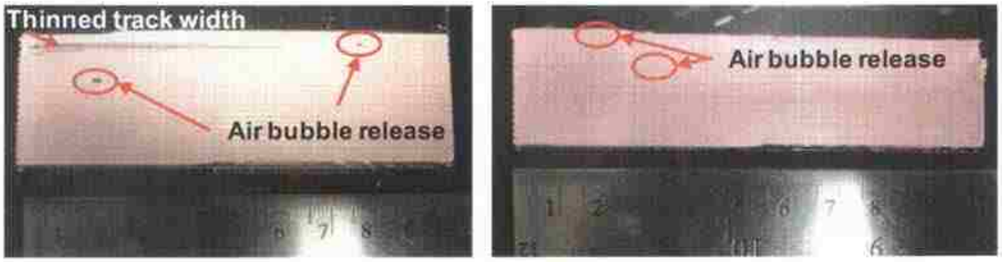

(a) (b)

Figure 17: Parts with defects due to air bubble release using (a) velocity controller with $u_{ref} = 0.01$ mm/s and (b) extrusion force controller with $F_{ref} = 630$ N.

The hybrid force-velocity controller discussed is implemented to account for air bubbles by using a conditional control structure. Plunger velocity control is used continually for steady-state extrusion to regulate the flow rate of each syringe; however, if the measured force drops to more than 20 N below the reference extrusion force, the control scheme switches to extrusion force control to regulate the extrusion force until the extrusion force is again within 20 N of the reference extrusion force, at which point plunger velocity control is re-enabled. This method allows the output flow rate to be quickly corrected within 400 ms (i.e., the closed-loop time constant of the extrusion force controller) following an air bubble release. Figure 18 demonstrates the use of this hybrid controller in the presence of an air bubble release. A serpentine pattern is deposited using the plunger velocity controller after injecting approximately 1 ml of air into the system. An air bubble release is encountered at 1.8 s, which causes a drop in the measured extrusion force past the 20 N threshold. After the extrusion force controller activates, only 0.2 s is required to fully recover since the reference plunger velocity is accelerated from 10 μm/s during steady-state to a maximum of 300 μm/s as the extrusion force controller adjusts the plunger velocity to maintain the reference extrusion force value. The table speed in this experiment is 12.7 mm/s and the air bubble release causes the extrusion force controller to activate within 200 ms. During this delay time, a 2.5 mm gap defect occurs due to the sudden loss of pressure within the syringe.

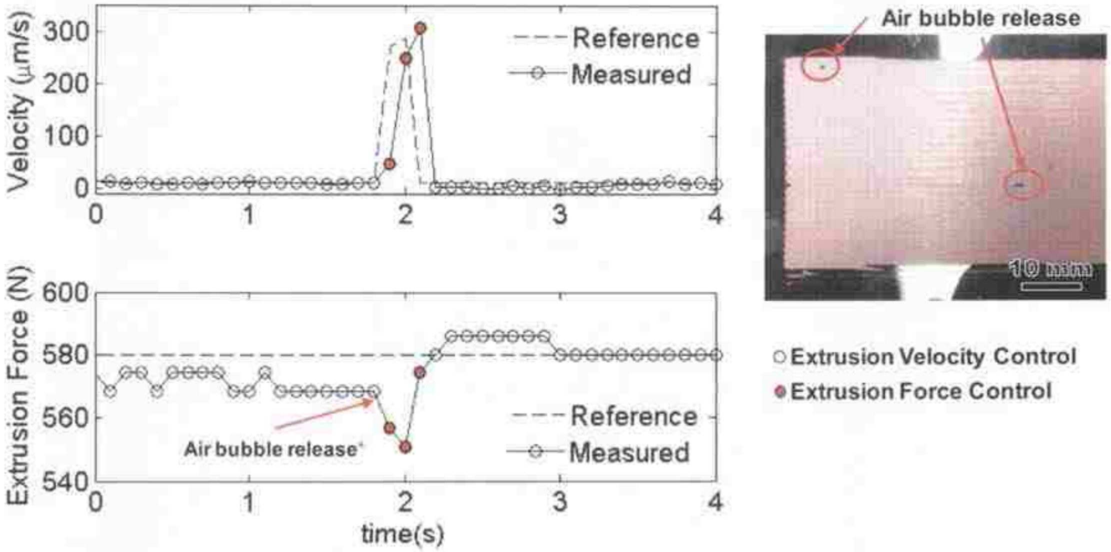

Figure 18: Measured extrusion force and plunger velocity for air bubble release when using the hybrid force-velocity controller.

The ability of the controller to use plunger velocity control is critical for fabrication of functionally graded parts since the flow rate of each material is regulated via the velocity of each plunger. The switching scheme described allows extrusion force control to be utilized for an instant following an air bubble release to correct the pressure within the syringe and regain the proper flow rate. Without air bubble release compensation (i.e., plunger velocity control alone), an entire part could be ruined if an air bubble release occurs during fabrication. While the hybrid force-velocity controller is not a substitute for proper paste preparation and loading techniques, it will minimize the defects associated with air bubble release during part fabrication.

6. DEMONSTRATION AND IMPLEMENTATION

The effectiveness of the hybrid controller was tested using an open-source tool path planning program, Skeinforge, to fabricate monolithic and functionally graded material parts. The files of tool paths generated by this path planning software were modified such that the FEF machine could interpret the tool path files (Figure 19). Process parameters such as extrudate bead width, standoff distance, and table velocity are determined through experimentation with the FEF machine. Extrusion-on-demand is regulated using the dwell-based start method (400 ms dwell) and the trajectory-based stop method (20 ms ahead of the stop point).

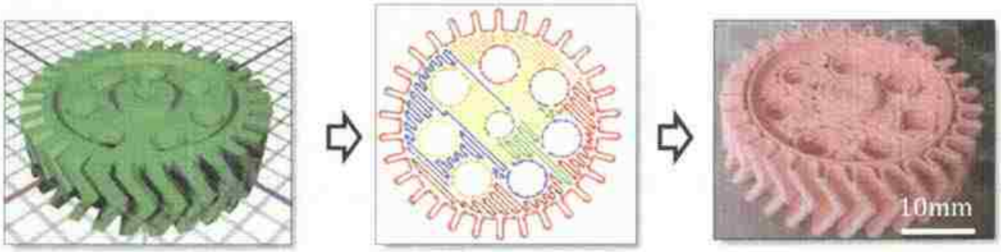

CAD Model Tool path FEF Part

Figure 19: Tool path generation flow chart for FEF part fabrication.

Single material parts are fabricated using alumina (Al_2O_3) paste in a freezing environment (-10°C) to demonstrate the ability of the hybrid controller to start and stop extrusion on demand for parts of complex shapes (Figure 20). Slope features as much as

45° from the vertical axis can be fabricated with no support structure, and the extrusion-on-demand control scheme allows the FEF machine to fabricate parts of varying size and complexity. The hybrid controller successfully switches between extrusion force control and plunger velocity control to maintain consistent extrusion width and no gaps in the tool path due to improper starting/stopping or due to air bubble release are observed during part fabrication.

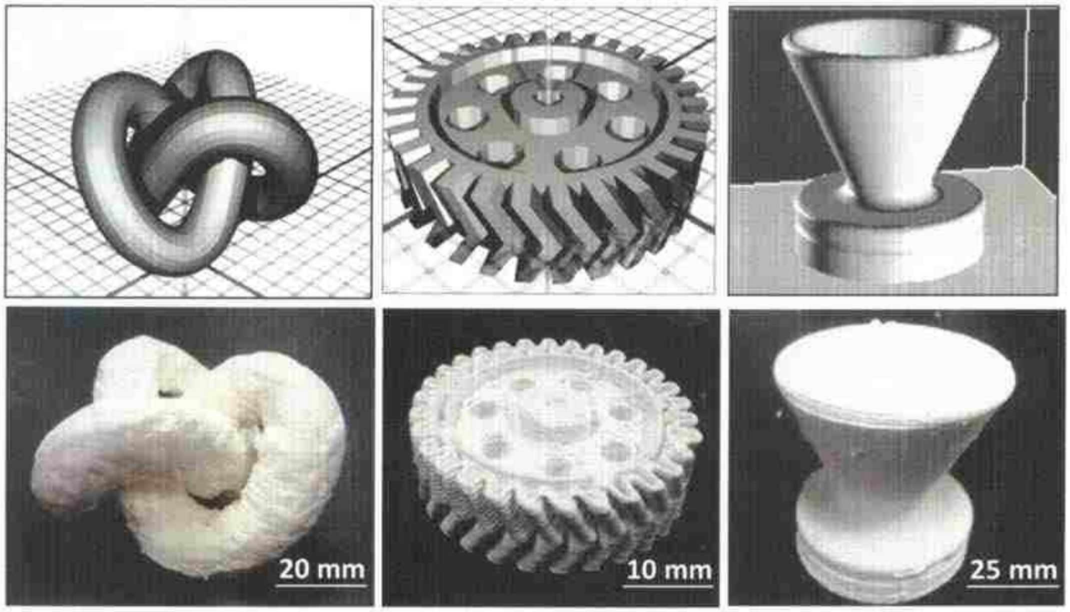

Figure 20: Sample parts made with Al_2O_3 paste.

Fabrication of functionally graded parts using the developed hybrid control scheme was demonstrated by fabricating a three-composition part (100% paste ‘A’, 50% paste ‘A’ and 50% paste ‘B’, 100% paste ‘B’) using two calcium carbonate ($CaCO_3$) pastes of pink and blue colors to represent two different materials (Figure 21). Three 3D models were created in a CAD software package to represent three compositions of paste ‘A’ and paste ‘B’. The tool path was generated for each component and a splicing program combined the tool paths into a single one with variable plunger velocities to account for multiple materials. The transport delay model was incorporated to account for change of compositions by shifting the reference plunger velocities ahead by the calculated transport delay. Paste compositions were successfully regulated from 100% paste ‘A’ to 100% paste ‘B’ using the plunger velocity controller for two syringes, and the extrusion force controller was utilized for start and stop commands in the tool path. The part is built on a layer-by-layer basis to form a radial gradient from the inner hemispherical region (paste 'A') to the outer block region (paste 'B') with a composition of 50% paste 'A' and paste 'B' between the two pure compositions.

Figure 21: Demonstration of fabricating a functionally graded material part using two $CaCO_3$ pastes of pink and blue colors.

7. SUMMARY AND CONCLUSIONS

A hybrid force-velocity controller has been developed to regulate the steady-state extrusion flow rate using a plunger velocity controller and to regulate extrusion-on-demand using an extrusion force controller for fabricating functionally graded material parts using the freeze-form extrusion fabrication process. Plunger velocity control is used normally for steady-state extrusion to regulate the flow rate of each syringe; however, the control scheme switches to extrusion force control when the measured force drops by more than a certain amount below the reference extrusion force. Extrusion force control is used in order to control extrudate start and stop properly despite the compressible behavior of the paste, which causes a slower transient response when using a plunger velocity controller. The extrusion force controller utilized for extrusion-on-demand operates in a closed-loop feedback control scheme; therefore, by selecting a "desired" closed-loop time constant, the delay time for trajectory start and stop is fixed and independent of paste properties. An added benefit of the hybrid controller is that the gap defects caused by the release of entrapped air bubbles are mitigated. The release of entrapped air bubbles within a part can be catastrophic for deposition-based additive manufacturing if the gap defect is large enough to cause structural failure. Minimizing these defects is essential since there is the potential for air bubble entrapment with any paste-deposition based process. Air bubble release compensation reduced the severity of defects caused by the release of an air bubble during part fabrication by utilizing the